J. Fluid Mech. (2001), *vol.* 441, *pp.* 293–314. Printed in the United Kingdom

On buoyancy-driven natural ventilation of a room with a heated floor

By CHARLOTTE GLADSTONE AND ANDREW W. WOODS

BP Institute for Multiphase Flow, University of Cambridge, Madingley Road, Cambridge CB3 0EZ, UK

(Received 5 June 2000 and in revised form 5 February 2001)

The natural ventilation of a room, both with a heated floor and connected to a cold exterior through two openings, is investigated by combining quantitative models with analogue laboratory experiments. The heated floor generates an areal source of buoyancy while the openings allow displacement ventilation to operate. When combined, these produce a steady state in which the air in the room is well-mixed, and the heat provided by the floor equals the heat lost by displacement. We develop a quantitative model describing this process, in which the advective heat transfer through the openings is balanced with the heat flux supplied at the floor. This model is successfully tested with observations from small-scale analogue laboratory experiments. We compare our results with the steady-state flow associated with a point source of buoyancy: for a given applied heat flux, an areal source produces heated air of lower temperature but a greater volume flux of air circulates through the room. We generalize the model to account for the effects of (i) a cooled roof as well as a heated floor, and (ii) an external wind or temperature gradient. In the former case, the direction of the flow through the openings depends on the temperature of the exterior air relative to an averaged roof and floor temperature. In the latter case, the flow is either buoyancy dominated or wind dominated depending on the strength of the pressure associated with the wind. Furthermore, there is an intermediate multiple-solution regime in which either flow regime may develop.

1. Introduction

When air inside a room is of different temperature and hence density from air outside, pressure gradients across any openings between the room and the exterior are produced. These may drive a net exchange flow which ventilates the room. With natural ventilation, the exchange flow is driven by these pressure differences alone. In forced ventilation, such as mechanical air-conditioning systems, the flow is also influenced by externally imposed pressure gradients. In the drive to construct low-energy, cost effective buildings which also provide a satisfactory environment for occupants in terms of indoor air quality and thermal comfort requirements, it is increasingly important for natural ventilation strategies to be incorporated.

Several key studies focus on combining simple analytical models with small-scale experiments to provide an insight into the fluid dynamics of ventilation flows in rooms (Linden 1999). Depending on the number and positions of the openings, and the dominant driving mechanism, the exchange of warm and cold air may involve mixing of the two fluids or simple draining with no mixing (Linden, Lane-Serff & Smeed 1990). The former process is termed mixing ventilation and the latter displacement

ventilation. The differences between these two processes are central when designing buildings which employ natural ventilation, depending upon the particular ventilation requirements. In a warm room linked to a cold exterior by a single opening located near the top of the room, mixing ventilation occurs. Cold exterior fluid enters and descends to the floor as a turbulent entraining plume (Linden 1999). When a single opening is located at the base of the room, a doorway exchange flow results (Dalziel & Lane-Serff 1991; Phillips & Woods 2000). If there are two openings at different levels in the room, either displacement or mixing ventilation occurs depending on the position of the lower opening. When this opening is at the base of the room, cold exterior fluid enters the room through it, displacing warm interior fluid up and out of the upper opening (Linden *et al.* 1990). If the lower opening is at some height above the floor, a hybrid form of natural ventilation occurs which involves both mixing and displacement (Gladstone & Woods 2000). Similar principles apply when gas leaks contaminate air in a room, again leading to different densities and pressure gradients inside and outside the room.

Displacement ventilation has also been explored extensively using full-sized room experiments, computational fluid dynamics (CFD) simulations and numerical modelling. Details of these and their applications can be found in Awbi (1991), Etheridge & Sandberg (1996) and Chen & Glicksman (2001). These approaches allow the monitoring or prediction of airflow patterns so that areas of thermal comfort and regions of contaminants can be ascertained. In particular, several investigations have focused on combining displacement ventilation, both natural and mechanically derived, with buoyancy sources such as those generated by cooled ceilings, to provide more efficient means of ventilating rooms (e.g. Alamdari *et al.* 1998).

These various approaches are also available as design tools (see Awbi 1991 and Allard 1998, for examples). There are several case studies where natural ventilation has been used successfully either as the primary form of ventilation where internal heat gains are small, or combined with more conventional air conditioning in buildings where higher internal gains occur (Allard 1998).

In order to minimize the operating costs of buildings, there has been considerable effort to examine the natural ventilation flow which results from a localized source of heat, e.g. a heater or radiator, in a room containing two openings (e.g. Thomas *et al.* 1963; Linden *et al.* 1990; Sandberg & Lindström 1990; Cooper & Linden 1996). These studies have revealed that in many situations, a two-layer stratification becomes established, with a hot upper layer venting from a high-level opening, and cold ambient air intruding through a low-level opening. However, in many modern office buildings solar radiation may pass through large glass panels, heating the floor and producing a distributed heat source. This is analogous to classical underfloor heating systems as originally pioneered by the Romans, and produces distributed rather than localized sources of heat. It is therefore of interest to examine the natural ventilation flows produced by an areal heat source in a room which is connected to an exterior by two openings. This forms the subject of the present paper. We develop an idealized model and laboratory experiments describing the heating of a room at the floor and the cooling of a room through or by the roof, in which the ventilation flow is driven by the temperature difference between the interior and exterior of the room. We consider the case where heat is provided to the room by conduction and distributed throughout the room by convective processes rather than radiation.

In § 2 we describe a scaled analogue experimental system to study the ventilation flow and temperature of fluid within a room heated by a distributed source and connected to a large exterior reservoir through two vents at different levels. Systematic

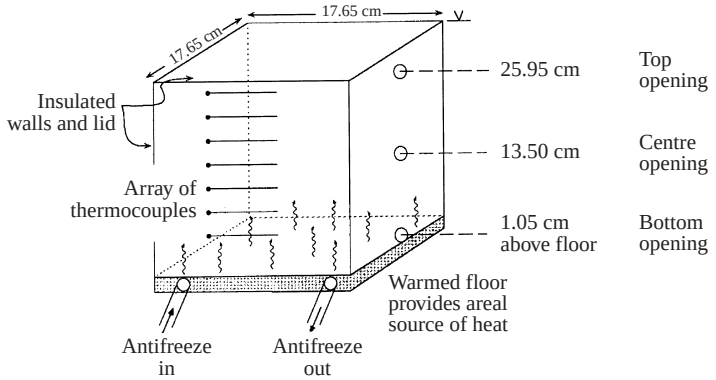

FIGURE 1. The room comprises a steel heating plate as the floor with three circular vents and an array of thermocouples placed at varying vertical heights in one sidewall. The floor provides an areal source of heat. This room is insulated where possible and placed in a large reservoir of water. Two of the three vents are opened during an experiment.

experiments are performed and the observations presented. In § 3 we develop a mathematical model describing these processes and our theoretical predictions are compared with the experimental results. The model is then generalized in § 4 to account for simultaneous heating by the floor and cooling through the ceiling, and also to include the role of a background wind which can generate an external pressure gradient across the room, again modifying or even dominating the background flow. The ventilation efficiency resulting from an areal source of buoyancy is compared to that resulting from a localized source of buoyancy. Conclusions and an example of the application of this modelling approach to a full-sized room are presented in § 5.

2. Experiments

2.1. *Method*

The analogue experimental system consists of a small Perspex tank (the room) of dimensions $17.65 \times 17.65 \times 28.7$ cm with circular openings in one wall, placed inside a large reservoir tank (the exterior), of dimensions $150 \times 75 \times 40$ cm. There are three openings, each with a diameter of 1.5 cm, and their midpoints at 1.05, 13.50 and 25.95 cm above the floor (figure 1). These are sealed by rubber stoppers which may be removed to initiate a ventilation flow. The floor of the room consists of a steel plate containing 1 cm diameter tubes spaced at intervals of 1.5 cm through which antifreeze is circulated by a Haake F6-C40 heater. This creates an areal or distributed buoyancy source which may be adjusted by changing the temperature of the circulating fluid. The floor is preheated to temperature T_F. The exterior reservoir is filled with cold water of temperature T_E, typically in the range 17.5 to 20.5 °C. The room is filled with warm fluid of temperature T initially chosen to equal T_F, so that the initial temperature difference between interior and exterior fluids, ΔT_0, ranges from 15 °C to 50 °C.

An experiment is commenced by removing stoppers from two of the three openings. Three series of experiments were conducted, all with the same values of ΔT_0. In Series 1, the bottom opening remained closed; in Series 2, the central opening was closed; and in Series 3, the top opening remained closed. Flow patterns were observed using the shadowgraph technique. The evolving temperature profile within the room was

monitored using seven Type K thermocouples placed at various heights above the floor of the room during Series 2 and 3, while an eighth thermocouple monitored the temperature of the reservoir, T_E. In Series 1, five thermocouples were placed inside the room while three were placed in the exterior reservoir to monitor the temperature of the fluid at and above the central (inlet) opening. Recordings were made every five seconds using Picolog software via a TC-08 cold junction. In each experimental series, T_F and T_E were varied. Twenty-eight experiments were performed and the temperature profile inside the room, $T(z)$, was recorded until the system reached steady state.

In order for small-scale experiments to provide a useful analogy to large-scale situations, dynamic similarity is required. For turbulent ventilation flows, the Reynolds number, *Re*, is the important dimensionless parameter,

$$Re = \frac{(g'H)^{1/2}H}{\nu} \tag{2.1}$$

where g' is the reduced gravity of the flow, H the characteristic lengthscale and ν the kinematic viscosity of the fluid. We use the subscript L to denote laboratory scale and the subscript F to denote full scale. While H_L is significantly less than H_F, using water in laboratory experiments to model air allows dynamic similarity to be achieved because $g'_L < g'_F$ and $\nu_L < \nu_F$ (Hunt & Linden 1999). For example, for a full-scale flow driven by a temperature difference of 10 °C, $g'_F \sim 0.4\,\mathrm{m\,s^{-2}}$ with $\nu_F \sim 10^{-5}\,\mathrm{m^2\,s^{-1}}$. If $H_F \sim 5\,\mathrm{m}$, this gives $Re_F \sim 10^5$. Using a small-scale experiment where $H_L \sim 0.3\,\mathrm{m}$ with a typical temperature difference $\Delta T_L \sim 30\,^\circ\mathrm{C}$, $g'_L = 0.1\,\mathrm{m\,s^{-2}}$ while $\nu_L \sim 10^{-6}\,\mathrm{m^2\,s^{-1}}$, leading to $Re_L \sim 10^4$.

In addition, the convective heat transfer needs to be considered and for this we compare the full-scale and laboratory-scale values of the Rayleigh number (Turner 1973),

$$Ra = \frac{g'H^3}{\kappa\nu} \tag{2.2}$$

where κ is the thermal diffusivity of the fluid. Using typical values of $\kappa_F \sim 10^{-5}$ and $\kappa_L \sim 10^{-7}$ gives $Ra_F \sim 10^{11}$ and $Ra_L \sim 10^{10}$. Under these conditions of high Rayleigh number convection, the conductive heat flux through the Perspex walls of the tank is only approximately 1% of the convective heat flux supplied by the floor and passing through the vents; hence to leading order it may therefore be neglected.

2.2. *Observations*

After removal of the stoppers, cold exterior fluid enters the room through the lower vent, displacing warm interior fluid upwards and out of the room through the upper vent. As the flow continues and the front between the warm and cold fluid ascends, the thermocouples in the room show a decrease in temperature sequentially from the bottom of the room to the top (figures 2*a* and 2*b*). However, as the lower layer deepens, convection driven by the heated floor becomes progressively more vigorous and the temperature in the room becomes more uniform with depth. A steady-state temperature, T_{SS}, which is very uniform throughout the room, is attained once this front reaches the top of the room, typically after about 30 minutes. The evolution of the temperature profile in the room also depends on the positions of the openings. Figure 2(*a*) shows the temperature changes in a room ventilated through the top and centre openings (Series 1), while in figure 2(*b*) the ventilation occurs through the top and bottom openings (Series 2). The displacement ventilation, which dominates both

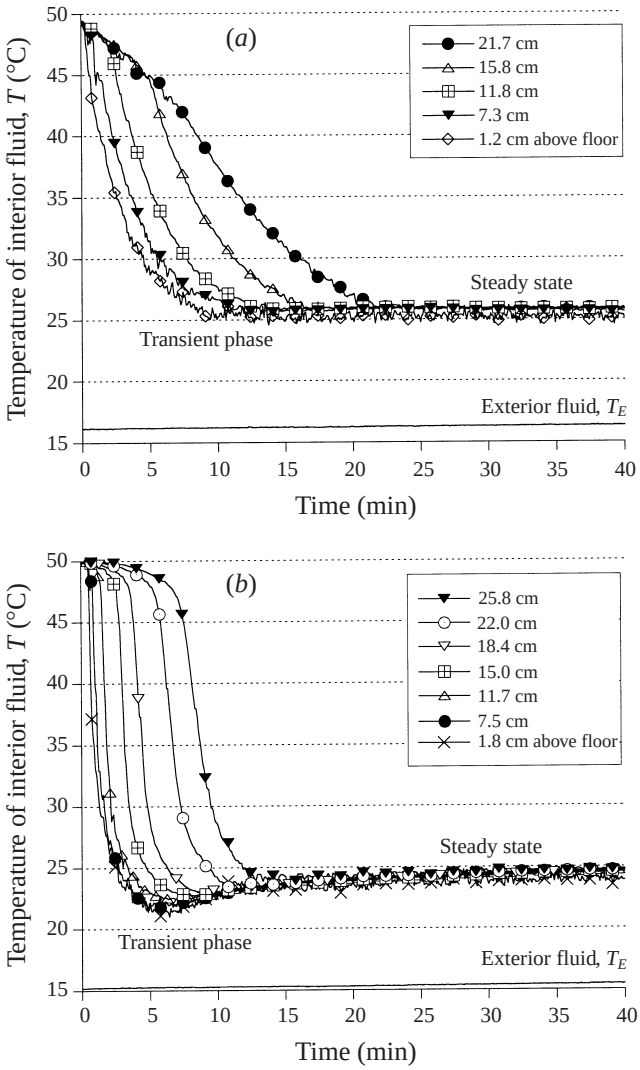

FIGURE 2. Temperature profiles of the fluid inside the room are captured by thermocouples at different heights during two steady-state experiments where $T_F = 50\,^{\circ}\mathrm{C}$. In (*a*) the top and central openings are employed, while in (*b*) top and bottom openings are employed. The steady-state regime is characterized by a uniform temperature throughout the room which remains constant while the temperature of the floor, T_F, and exterior fluid, T_E, are held constant.

experiments during early stages, is stronger when the distance between the openings is large, to the extent that the temperature of the room dips to a few degrees below T_{SS} before the thermal convection associated with heating of the floor eventually drives the system towards the steady state (figure 2*b*). The steady-state temperature, T_{SS}, depends on the floor temperature, T_F, and the positions of the two openings (figure 3). In all three configurations of openings, the higher the floor temperature, T_F, the higher the value of T_{SS}.

Shadowgraphs reveal the different flow patterns resulting from placement of the inflow vent at mid level (Series 1, figure 4*a*) or at low level (Series 2, figure 4*b*). The plume of cold exterior fluid entering the room through the centre opening (figure 4*a*)

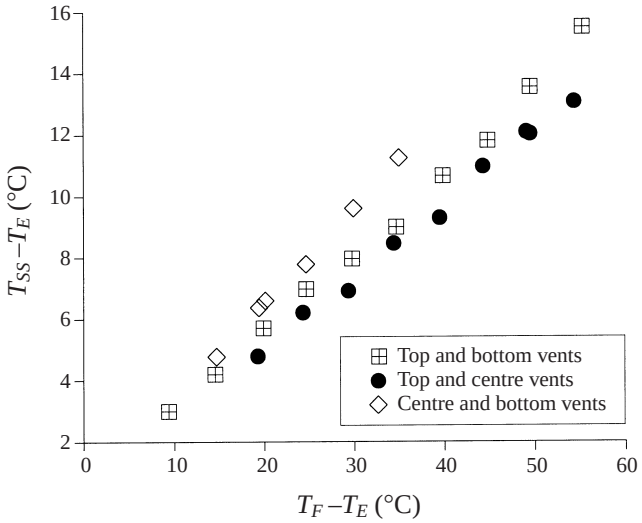

FIGURE 3. Steady-state measurements using varying values for the floor, T_F, and exterior, T_E, temperatures suggest that for a given configuration of vents, T_{SS} increases approximately linearly with T_F. Repeated experiments indicate reproducibility to within 4%.

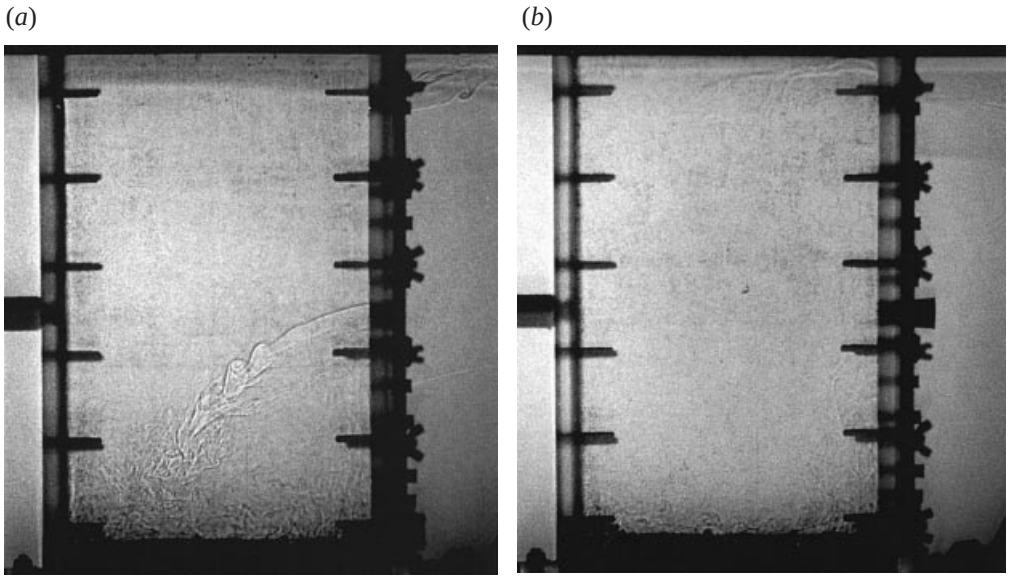

FIGURE 4. Shadowgraphs showing the steady-state dynamics in a room with a heated floor combined with displacement ventilation through two openings. For both experiments, $T_F = 50\,^{\circ}\mathrm{C}$ and $T_E = 15\,^{\circ}\mathrm{C}$. In (*a*) cold exterior fluid enters the room through the mid-level vents and descends to the floor while hot interior fluid exits the room through the high-level vent. In (*b*) cold exterior fluid enters through the low-level vent, but is dispersed by the vigorous convection arising from the heating plate. Hot interior fluid exits through the high-level vent.

descends to the floor, entraining the warmer interior fluid of temperature T. Vigorous convection from the heated floor is evident. Warm interior fluid exits through the top opening. When the top and bottom openings are used, exterior fluid enters through the bottom opening and initially spreads radially as a gravity current. As this fluid

mixes with the plumes of hot fluid rising from the heated floor, the gravity current becomes dispersed. These plumes of hot fluid can be observed rising through the room to the very top (figure 4*b*).

3. Modelling steady state

3.1. *Model*

We now develop a leading-order model of the heating and flow observed in these steady-state experiments. As the Rayleigh number, *Ra*, associated with a heating plate is large (Turner 1973) we assume that the convection is turbulent and the fluid in the room is well-mixed. Furthermore, since the temperature in the room is elevated relative to the exterior, we expect dense exterior fluid to enter the room through the lower opening. This then displaces the warmer and hence lighter fluid out of the room through the upper opening. For openings of small vertical dimension compared to their separation, the buoyancy-driven volume flux through each of the openings during displacement, Q_V, is given from dimensional analysis by the relation (cf. Linden *et al.* 1990)

$$Q_V = \left[\left(\frac{g(\rho_{ext} - \rho_{int})}{\rho_{int}}\right)\frac{h}{2}\right]^{1/2} cA_H \tag{3.1}$$

where g is the acceleration due to gravity, h the distance between the midpoints of the upper and lower openings, ρ_{ext} and ρ_{int} are the densities of the exterior and interior fluids respectively, A_H is the average area of the openings and c is a constant. This constant is related to the loss of energy associated with flow through an opening. For a smoothly evolving flow with no energy loss, $c = 1.0$; with a sudden opening which causes the flow to expand sharply, $c = 0.5$ (Batchelor 1967).

The heat flux supplied by the hot floor may be estimated from previous work on the turbulent convection generated by horizontal heated plates. Extensive studies include those by Townsend (1959), exploring conduction and convection from a single heated plate, and a review of both single- and double-plate experiments by Denton & Wood (1979). These studies found that, for Rayleigh numbers of order 10^7–10^9, if the heating plate has temperature T_F and the fluid in the room has temperature T, the heat flux supplied to the room by the floor, Q_H, is given by the approximate empirical relation

$$Q_H = J(T_F - T)^{4/3} = \lambda A_R \left(\frac{\alpha g}{\kappa\nu}\right)^{1/3} \rho C_p \kappa (T_F - T)^{4/3} \tag{3.2}$$

where A_R is the area of the room, ρ and C_p are the density and heat capacity of the fluid respectively, λ is a dimensionless constant which characterizes the heating from the plate and α represents the expansion coefficient (Turner 1973; Denton & Wood 1979). Empirical measurements show that $\lambda = 2^{4/3} c_q$ where c_q is the heat transfer coefficient (Townsend 1959). More recent detailed experimental studies have identified that there are in fact different regimes of turbulent thermal convection, termed soft and hard turbulence depending on the Rayleigh number; experimentally, the transition from soft to hard occurs as the Rayleigh number increases to very large values, $Ra > 10^9$ (Castaing *et al.* 1989). At this transition there is a change in the exponent relating the heat flux, Q_H, to temperature, $(T_F - T)$, from 4/3 to 9/7. However, we find that the parameterization of the heat flux associated with soft turbulence (equation (3.2), and Denton & Wood 1979) is extremely accurate for the present study (cf. Kerr *et al.* 1990).

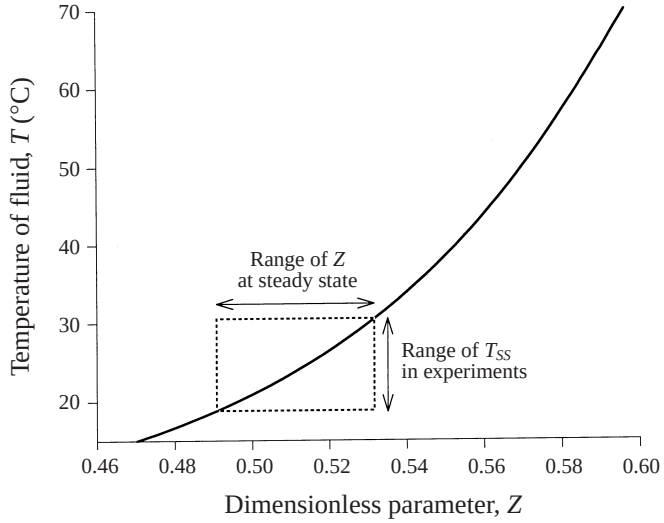

FIGURE 5. Plotting Z as a function of T reveals that in the range of conditions reached at steady state, the dependence is weak. This curve is evaluated using equation (3.6).

The global conservation of thermal energy in the room requires that in steady state, the temperature in the room, T_{SS}, is given by the balance between the heat flux from the plate, Q_H, and the heat loss due to the exchange flow with the exterior, Q_V,

$$Q_H = \rho C_p (T_{SS} - T_E) Q_V. \tag{3.3}$$

It is convenient to use a dimensionless temperature, θ, defined in terms of the floor temperature and the exterior temperature,

$$\theta = \frac{T_{SS} - T_E}{T_F - T_E} \tag{3.4}$$

so that (3.3) reduces to the algebraic relation

$$(1 - \theta)^{4/3} = Z \theta^{3/2} \tag{3.5}$$

where

$$Z = \left(\frac{c}{\lambda}\right) \frac{A_H}{A_R} \left(\frac{g^{1/2} \alpha^{1/2} \nu}{\kappa^2}\right)^{1/3}. \tag{3.6}$$

Z is a dimensionless parameter incorporating the coefficients from the convection driven by heating at the floor and also the exchange flow through the openings. Z does in fact depend on the fluid temperature although this dependence is relatively weak for conditions which develop during the steady-state regime (figure 5). For large Z, corresponding to the case of large openings, there is a relatively rapid displacement flow and $\theta \to 0$, the temperature of the exterior fluid. In contrast, for small Z, corresponding to small openings, there is a relatively slow flow and hence rapid heating by the convection, so that $\theta \to 1$, the temperature of the heating plate.

3.2. *Comparison with experiments*

In order to generate quantitative theoretical predictions of T_{SS}, values for the constants c and λ are required. Calibration experiments for our apparatus are presented in the Appendix. Transient displacement ventilation experiments for our system give

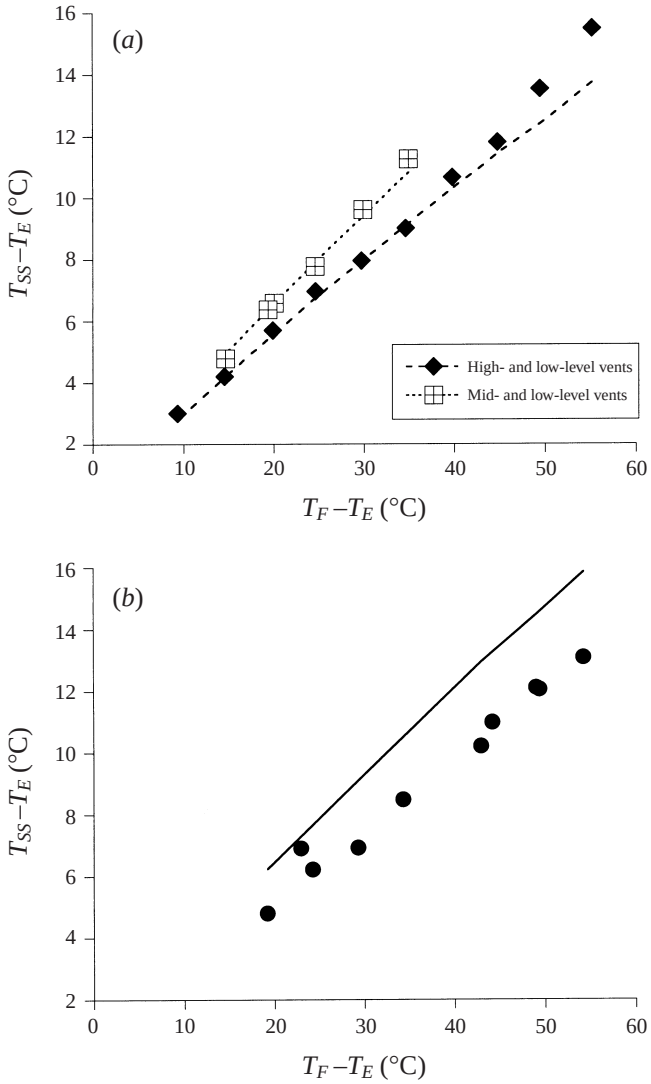

FIGURE 6. Theoretical predictions (lines) and experimental observations (symbols) of the steady-state temperature, T_{SS}, to which the fluid inside the room evolves, are shown using (*a*) high- and low-, or mid- and low-level vents, and (*b*) high- and mid-level vents.

the result that $c = 0.98 \pm 0.15$ while transient heating experiments indicate that $\lambda = 0.166 \pm 0.003$.

The observations and theoretical predictions of the steady-state temperature, T_{SS}, are in very good accord for experiments in which the top and bottom, or central and bottom openings are used, i.e. those configurations where cold exterior fluid enters at the base of the room (figure 6*a*).

When the inflow vent is placed at mid-level, experimental steady-state temperatures are approximately 10% less than theoretical predictions (figure 6*b*). With this configuration of vents, exterior fluid entering the room entrains hot interior fluid as it descends towards the floor (figure 4*a*). On reaching the floor this fluid is warmer than T_E and thus the transfer of heat from the heating plate is reduced. Consequently the

interior temperature of the room is suppressed, and so is the exchange flow through the openings. This in turn reduces the flux of further T_E fluid entering the room. The overall result is a lower steady-state temperature compared to that achieved when the inflow vent is situated at the base of the room. Nonetheless, the model provides a good leading-order description of the process.

4. Generalization of the model

The model developed to describe the experiments is idealized. Amongst other simplifications, it assumes that there is no external wind; that the density of the fluid outside the room is uniform; that the heat source at the floor is derived from a plate of uniform temperature; and that the ceiling and walls of the room are insulating. In practice, some or all of these simplifications may not apply, so we now generalize the model to examine how (i) an external wind, and (ii) a cooled ceiling, may affect the results described in § 3, and (iii) to provide a simple comparison between the natural ventilation resulting from distributed and point-source heating.

4.1. *Heated floor and cooled ceiling*

In some modern buildings, atria or hallways are connected to the main part of the building by several high- and low-level openings. Such atria often include many glass panels which will admit solar radiation. This may ultimately warm up the floor producing a distributed heat source, while the glass ceiling may be cooled from the exterior and thus act as a heat sink. Alternatively, excess heat in rooms may be removed by radiant chilling systems in which coolant circulates through an array of pipes in the ceiling. It is therefore of interest to examine the flow which develops in a room with a cooled ceiling and a heated floor.

In this example, a room with temperature T is connected to an adjacent building of temperature T_A by high-level and low-level openings (figures 7*a* and 7*b*). In this idealized model, the adjacent building is sufficiently large that over the scale of the ventilation flow T_A is constant. We assume the heated floor has temperature T_F while the chilled ceiling has temperature T_C ($\leqslant T$). Following the experiments and model presented in § 2 and § 3 and to illustrate the process, we parameterize the heat flux from the floor to the interior of the room, Q_F, in the form

$$Q_F = J_F(T_F - T)^{4/3} \tag{4.1}$$

where J_F is given by (3.2) and evaluated at temperature T_F. Correspondingly, the heat flux supplied to the ceiling from the room, Q_C, is given by

$$Q_C = J_C(T - T_C)^{4/3}. \tag{4.2}$$

Again, J_C is given by (3.2) and evaluated at temperature T_C. If the room temperature T is greater than that of the adjacent building T_A, then there will be an inflow through the lower vent and outflow through the upper vent (figure 7*a*). Conversely, if T is smaller than T_A, there will be outflow through the lower vent and inflow through the upper vent (figure 7*b*). This volume flux, Q_V, may be parameterized as for the displacement flow described in § 3,

$$Q_V = F(T - T_A)^{1/2}, \tag{4.3}$$

for the case in which the room is hotter than the adjacent building, where $F = cA_H(gh/2)^{1/2}$, A_H is the geometric mean of the area of the two openings, h is the

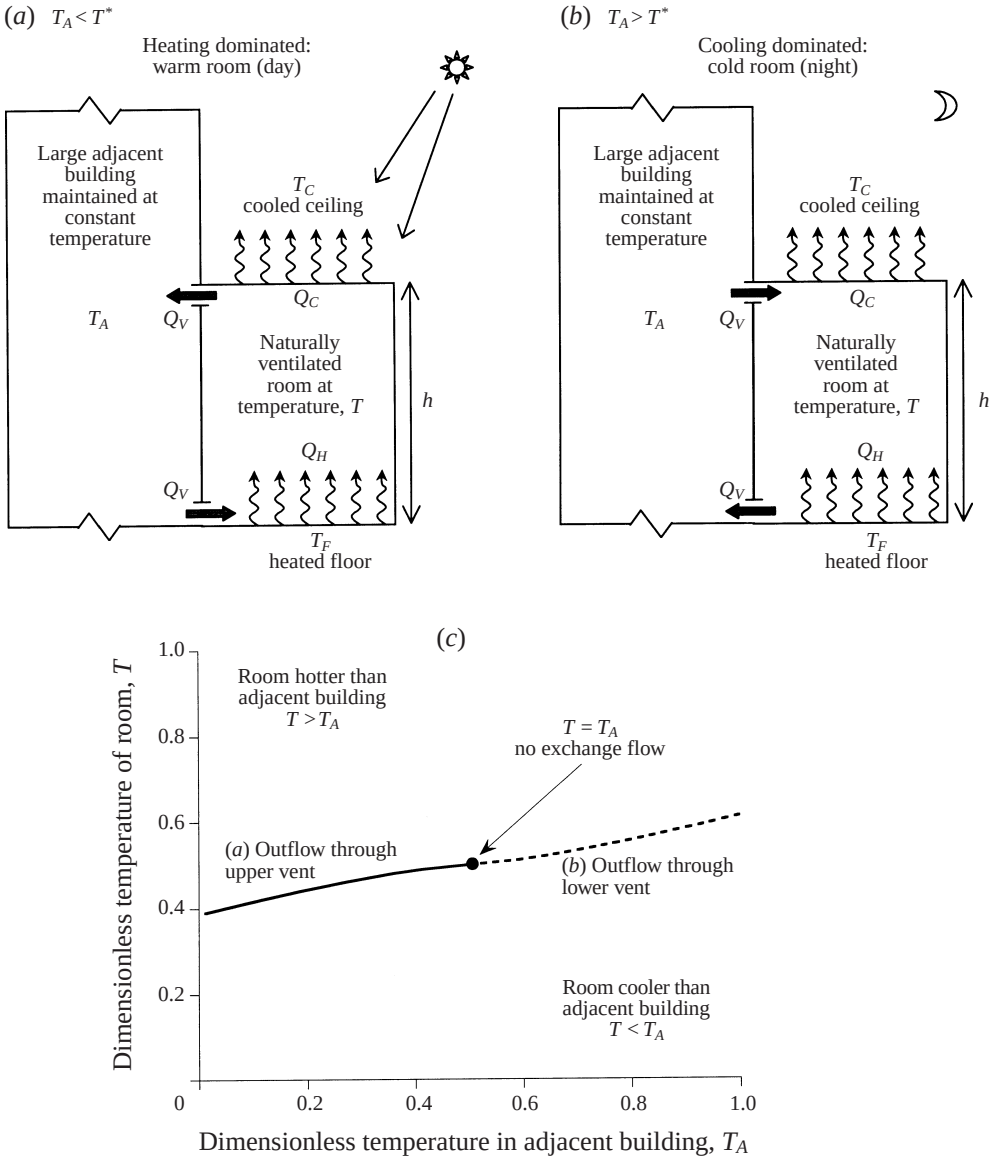

FIGURE 7. Schematic showing the natural ventilation of a room at temperature T with a heated floor and chilled ceiling at temperatures T_F and T_C respectively, and joined by high- and low-level openings to a large adjacent building at temperature T_A: in (*a*) outflow occurs through the high-level vent and inflow through the low-level vent while in (*b*), the reverse applies. The conditions under which inflow or outflow may apply are plotted in (*c*) by the solid curve. Above the curve outflow occurs through the upper vent as shown in (*a*); below the curve outflow is through the lower vent in (*b*). At the curve itself, $T_A = T^*$ so there is no exchange flow.

vertical distance between the openings and c is a constant (Linden *et al.* 1990). The heat flux associated with this mass flow, Q_H, is

$$Q_H = Q(T - T_A)^{3/2} \tag{4.4}$$

where $Q = \rho C_p F$. By balancing these three heat fluxes of (4.1), (4.2) and (4.4), we deduce that in steady state, if the room is hotter than the adjacent building, then the

temperature of the room is given by the relation

$$J_F(T_F - T)^{4/3} = J_C(T - T_C)^{4/3} + Q(T - T_A)^{3/2}. \tag{4.5}$$

The limiting condition in which there is no flow through the openings occurs if the temperature of the fluid in the adjacent room, T_A, equals the critical temperature, T^*,

$$T_A = T^* = \frac{J_F^{3/4} T_F + J_C^{3/4} T_C}{J_F^{3/4} + J_C^{3/4}}. \tag{4.6}$$

If $T_A < T^*$ then the atrium is indeed warmer than the adjacent room and there is outflow from the upper vent (figures 7*a* and 7*c*). However, if $T_A > T^*$, then the flow reverses (figures 7*b* and 7*c*), and the steady-state heat balance takes the form

$$J_F(T_F - T)^{4/3} = J_C(T - T_C)^{4/3} - Q(T_A - T)^{3/2}. \tag{4.7}$$

These results are summarized in figure 7(*c*), in which we illustrate the variation of the dimensionless temperature in the room, $(T - T_C)/(T_F - T_C)$, as a function of the dimensionless temperature of the adjoining building, $(T_A - T_C)/(T_F - T_C)$. The direction of the flow in both situations $T_A > T^*$ and $T_A < T^*$ is also indicated.

4.2. *The effect of wind*

The steady-state flow within a ventilated room which is heated by an underfloor heating system may change dramatically if there is an external pressure difference between the two openings. Such a pressure difference may arise from a background wind (Hunt & Linden 1999) and acts against or in addition to the pressure difference associated with the temperature and hence density contrast between the fluid inside the building relative to that outside (figures 8*a* and 8*b*).

In this example, we assume that the heated floor has temperature T_F and provides a heat flux, Q_F,

$$Q_F = J(T_F - T)^{4/3} \tag{4.8}$$

where the room has temperature T. The pressure difference between the upper and lower vents associated with the wind is Δp, and the pressure difference associated with the buoyancy contrast between the interior and exterior fluid is $g\alpha(T - T_E)h$, where h is the distance between the openings. If the flow through the openings is dominated by the buoyancy forces (figure 8*a*), then the outflow through the upper vent, Q_V, equals that through the lower vent, and is given by

$$Q_V = cA_H \left(\frac{g\alpha(T - T_E)h - \Delta p}{2} \right)^{1/2}. \tag{4.9}$$

Combining (4.8) and (4.9), we deduce that the steady-state heat balance between the floor heating and the ventilation flow has the form

$$J_F(T_F - T)^{4/3} = \rho C_p A_H \left(\frac{g\alpha(T - T_E)h - \Delta p}{2} \right)^{1/2} (T - T_E). \tag{4.10}$$

This relation may be expressed in the dimensionless form

$$(1 - \theta)^{4/3} = Z\theta(\theta - p^*)^{1/2} \tag{4.11}$$

where θ denotes the dimensionless room temperature $\theta = (T - T_E)/(T_F - T_E)$. Here, the two control parameters are $Z = \rho C_p A_H (g\alpha h/2)^{1/2}/J_F$ and $p^* = \Delta p/(g\alpha(T_F - T_E))$.

Equation (4.11) only admits solutions θ in the range $1 < \theta < 0$ if $p^* < 1$. In this

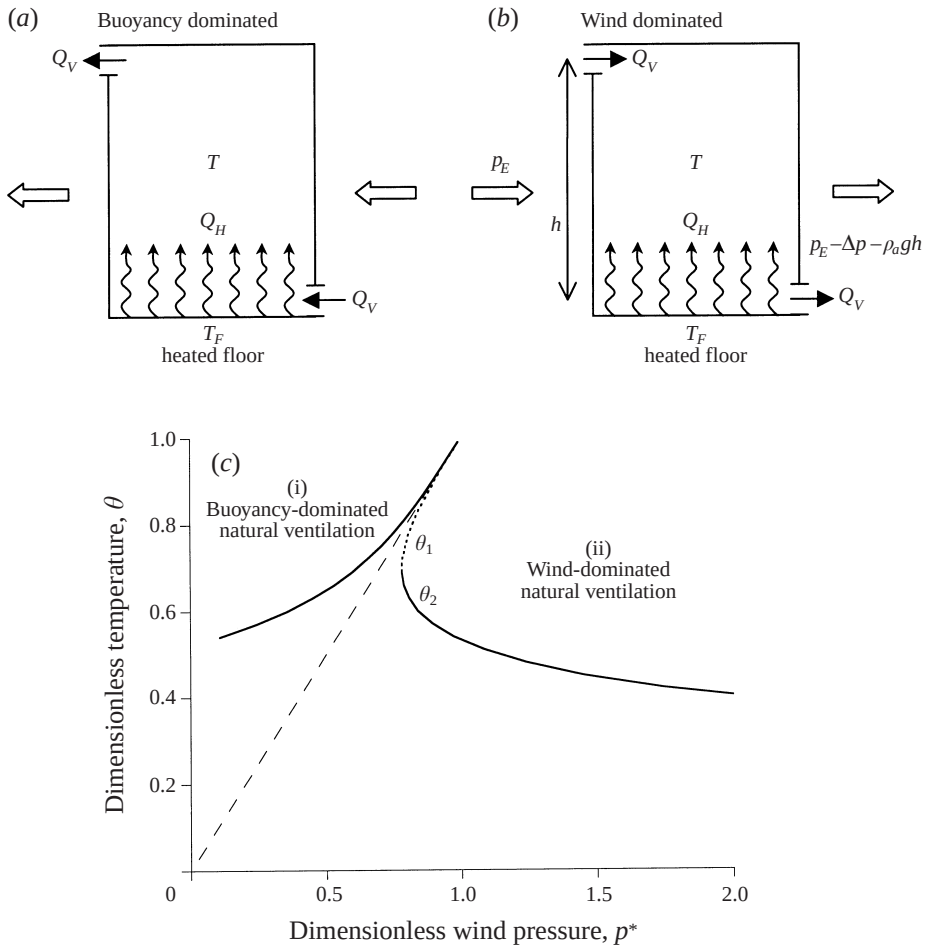

FIGURE 8. Schematics illustrating the effect of wind on a room with a heated floor and two openings to a cold exterior. In (*a*), the wind assists ventilation, while in (*b*) the wind opposes (cf. Hunt & Linden 1999). In (*c*) the dimensionless temperature of a room, θ, plotted with dimensionless wind pressure, p^*, shows the buoyancy-dominated or wind-dominated natural ventilation which may occur, with a dashed line separating these two regimes. Under wind-dominated conditions a slow exchange flow (θ_1; dotted curve) or fast exchange flow (θ_2; solid curve) may arise. As θ_1 is unstable there is the possibility for oscillations to occur.

regime the buoyancy forces can dominate the background pressure gradient associated with the wind. The variation of θ with p^* is illustrated in figure 8(*c*) which shows that there is a unique solution for θ for the buoyancy-dominated flow for each value of p^* (figure 8*c*, i). In the case $p^* > 1$, the background pressure dominates the buoyancy producing wind-dominated natural ventilation, and the flow reverses (figure 8*c*, ii), so that the temperature is given by the relation

$$(1-\theta)^{4/3} = Z\theta(p^* - \theta)^{1/2}. \tag{4.12}$$

However, equation (4.12) also has solutions for $1 > p^* > p_C$ where $0 < p_C < 1$ is the critical wind pressure difference required to overcome the buoyancy forces. In the region $p_C < p^* < 1$, there are in fact two possible wind-dominated solutions: a

relatively slow exchange flow from a warm room, $\theta = \theta_1$ (marked by a dotted curve; figure 8*c*), and a relatively fast exchange flow from a colder room, $\theta = \theta_2 (< \theta_1)$ (a solid curve; figure 8*c*). For $p^* > 1$, there is a unique wind-driven regime which corresponds to the continuous extension of the fast flow regime.

The slow flow regime, θ_1, for $p_C < p^* < 1$ is in fact unstable (dotted curve; figure 8*c*). This may be seen by considering the evolution of the system away from the equilibrium point using the relation for the bulk conservation of heat in the room,

$$\gamma \frac{\mathrm{d}\theta}{\mathrm{d}t} = (1-\theta)^{4/3} - Z\theta\left(p^* - \theta\right)^{1/2} \tag{4.13}$$

where $\gamma = \rho C_p h / J_P$. If we denote the steady-state temperature as $\theta = \theta_0$, then a small perturbation, $\varepsilon\phi(t)$, from this steady state, $\theta \to \theta_0 + \epsilon\phi$, evolves according to the relation

$$\gamma \frac{\mathrm{d}\phi}{\mathrm{d}t} = \phi \left[-\tfrac{4}{3}(1-\theta_0)^{1/3} - Z(p^* - \theta_0)^{1/2} + \frac{Z\theta_0}{2}(p^* - \theta_0)^{-1/2} \right]. \tag{4.14}$$

The term in square brackets is positive for $\theta_0 = \theta_1$ and negative for $\theta_0 = \theta_2$, so that the slow, high-temperature region is unstable, ($\theta_0 = \theta_1$) while the fast, low-temperature region is stable ($\theta_0 = \theta_2$).

The existence of both steady buoyancy-dominated and wind-dominated flow regimes which occur in the situation $p_C < p^* < 1$ may lead to difficulties in regulating the temperature regime of a room using a thermostatic control system. Multiple steady states have also been reported when natural ventilation is driven by a point source of buoyancy (Holford & Hunt 2000) or affected by an imposed wind (Hunt & Linden 2000).

4.3. *Comparison with a localized source of heat*

The displacement ventilation through openings associated with a localized or point source of heat or buoyancy has been explored extensively using a variety of techniques (see Etheridge & Sandberg 1996). This type of heat source generates a turbulent buoyant plume producing a localized convective flow with a sharp interface which develops at some height z above the floor, between the inflow and outflow vents (Thomas *et al.* 1963; Linden *et al.* 1990). A layer of hot air forms above the interface with colder ambient air confined to below the interface. If the upper hot layer of the room has buoyancy $g_1' = g\Delta T_1 / T_E$, then the volume flux of air through the room, driven by the natural ventilation, Q_{1V}, is

$$Q_{1V} = cA_H \left[g \frac{\Delta T_1}{T_E} \left(\frac{H-z}{2} \right) \right]^{1/2} \tag{4.15}$$

where H is the depth of the room, A_H the average area of the openings, c a constant and ΔT_1 the temperature difference between the hot layer and the exterior fluid of temperature T_E. Thus the heat flux, Q_{1H}, has the value

$$Q_{1H} = \rho C_p \left(\frac{\Delta T_1}{T_E} \right)^{3/2} \frac{g^{1/2}(H-z)^{1/2}}{2^{1/2}}. \tag{4.16}$$

The height of the interface, z, depends on the geometry of the openings, the depth of the room, and the detailed initial condition of the heat source, with the interface ascending as the size of the openings increases (Linden *et al.* 1990).

In contrast, here we have found that for a given heat flux supplied from an areal

source at the base of the room, a well-mixed layer forms throughout the room of buoyancy $g_2' = g\Delta T_2/T_E$ where ΔT_2 is the temperature difference between the room and exterior. Now, the volume flux, Q_{2V}, associated with the natural ventilation flow is

$$Q_{2V} = cA_H \left(g \frac{\Delta T_2}{T_E} \frac{H}{2} \right)^{1/2} \tag{4.17}$$

while the heat flux, Q_{2H}, is

$$Q_{2H} = \rho C_p \left(\frac{\Delta T_2}{T_E} \right)^{3/2} \frac{g^{1/2} H^{1/2}}{2^{1/2}}. \tag{4.18}$$

If the heat fluxes supplied to the distributed and localized sources of heating are identical, then it follows from the above results of equations (4.15) and (4.17) that the ratio of the temperature of the heated layers produced by the point source heating compared to the areal source heating is

$$\frac{\Delta T_1}{\Delta T_2} = \left(\frac{H}{H - z} \right)^{1/3}. \tag{4.19}$$

This indicates that with point source heating, the region of the room which is heated becomes hotter than with areal source heating. However, during point source heating there is a layer near the floor which is not heated whereas areal heating provides warming of the entire room.

Furthermore, the ratio of the volume flux of air circulating through the room and openings associated with the natural ventilation flow is

$$\frac{Q_{1V}}{Q_{2V}} = \left(\frac{H - z}{H} \right)^{1/3}. \tag{4.20}$$

This shows that when a room is naturally ventilated by an areal source of heat, there is faster circulation of air through the room, depending on the height of the interface produced from the localized source of heating (cf. Linden *et al.* 1990). Thus areal heating provides more effective ventilation than point source heating for a given heat flux.

5. Conclusions

This experimental and theoretical study has shown that fluid in a warm room which is heated by an areal source at the base of the room, and is connected to a cold exterior through two openings becomes well-mixed and drives a net ventilation flow with the exterior fluid. Similarly, fluid in a room which is chilled by an areal air conditioning unit from the ceiling will also become well-mixed with an approximately uniform interior temperature, when joined to a warmer exterior by vents through which displacement ventilation may occur.

We have developed an analogue experimental system and measurements of the steady-state temperature of this system, T_{SS}, are in good accord with the predictions of a new model based on the conservation of heat. The steady-state temperature depends primarily on the temperature of the floor, T_F, and exterior fluid, T_E, as well as the lengthscale of the openings compared to that of the room. Extension of the model to account for an externally imposed wind illustrates that the wind-dominated and buoyancy-dominated flow regimes overlap, leading to the possibility of multiple steady flow regimes under certain operating conditions. This study indicates that the

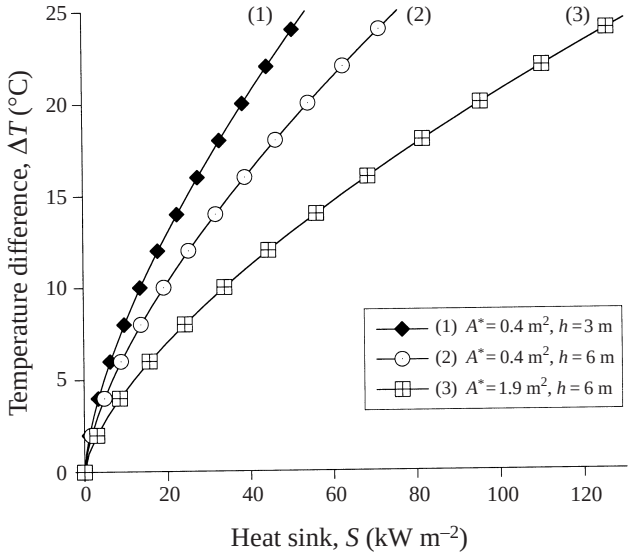

FIGURE 9. A simple application of the model to a chilled room joined by a low-level door and high-level window to a warm exterior illustrates the dependence of the temperature difference between the interior and exterior, ΔT, on the strength of the heat sink, S, the height of the room, H, and the effective area of the inflow and outflow vents, A^*.

natural ventilation produced by areal heating or cooling contrasts with that produced by a localized source. In the former, the interior temperature is approximately uniform and for a given heat flux the associated ventilation flow is larger. In the latter, the interior becomes strongly stratified in temperature and the resultant flow for a given heat flux is smaller.

Our new model provides insight into the natural ventilation regimes which may develop in some modern buildings. As a simple example of the application of the model, consider a room with high (e.g. a window) and low (e.g. a door) level vents and subject to radiant cooling through the ceiling which produces a heat sink. With a vertical distance between the openings of h, the temperature difference between the cooled room and warm exterior, ΔT, resulting from the heat sink, S, per unit area, is given by

$$A^*(g\alpha\Delta T h)^{1/2}\Delta T\rho C_p = S. \tag{5.1}$$

The empirical constant λ included in the steady-state model described by equation (3.2) may be omitted in this example because heating is not provided by a conducting plate. Similarly, the constant c describing the pressure loss through the openings is also removed because we now employ the effective area of the openings, A^*. This is defined as (Linden 1999)

$$A^* = \frac{c_d a_t a_b}{[0.5((c_d^2/c_e)a_t^2 + a_b^2)]^{1/2}} \tag{5.2}$$

where a_t and a_b are the areas of the top and bottom openings respectively. A discharge coefficient describing the outflow through the top vent c_d is included. Theoretical and experimental investigations show that at high Reynolds number, a value for c_d of 0.6 is appropriate (Etheridge & Sandberg 1996). Also, an expansion coefficient describing the pressure loss during inflow through the bottom vent c_e, is employed. We use a value of 0.5, denoting a sharp expansion at the inlet (Batchelor 1967). We include equation

(5.2) in this example because it allows the incorporation of discharge and expansion coefficients, both widely used in the ventilation industry. The following typical values for air are taken (Batchelor 1967; Weast 1987): expansion coefficient, $\alpha = 3.5 \times 10^{-3}$; heat capacity, $C_p = 1012\,\mathrm{J\,kg^{-1}}$; density, $\rho = 1.2\,\mathrm{kg\,m^{-3}}$ and gravitational constant, $g = 9.81\,\mathrm{m\,s^{-2}}$.

A window of dimension $1 \times 0.5\,\mathrm{m}$ is selected for the high-level vent and a door of dimension $2 \times 0.75\,\mathrm{m}$ for the low-level vent. We plot three curves illustrating the variation of the cooling of the room, ΔT, as the strength of the heat flux removed by the cooled ceiling, S, increases. The curves correspond to (1) a room found in a typical house with height $H = 3\,\mathrm{m}$ and one window and one door open, (2) a taller room, for example a hall, with height $H = 6\,\mathrm{m}$ and the same openings and (3) the tall room with height $H = 6\,\mathrm{m}$, but this time with two doors and six windows open (figure 9).

These curves illustrate the effect of the distance between the openings, the size of the openings, and strength of the cooling system on the temperature difference between the cooled room and warm exterior. For a given rate of heat extraction, doubling the vertical distance between the openings, h (curves 1 and 2; figure 9), causes a decrease in the amount of cooling of the room. The greater vertical distance between the window and the door leads to a faster flow for a given temperature difference and hence to maintain the same heat flux, the temperature difference decreases. Enlarging the openings and thus the effective area A^* (curves 2 and 3; figure 9), produces a larger decrease in the amount of cooling. This is caused by a greater volume flux through the vents. These effects become more pronounced with increasing strength of the cooling system.

There is a substantial amount of further investigation required on this subject. We have attempted to describe the key features of the steady-state regime resulting from distributed heating; analysis of the transient phase would also be desirable. In addition, the effects of radiation have not been considered here and could form the basis for additional research.

This study was funded by the Built Environment Programme of the Engineering and Physical Sciences Research Council. C.G. is also funded by the BP Institute for Multiphase Flow and the Isaac Newton Trust. We thank Jeremy Phillips and Brian Duddell for experimental assistance and Gary Hunt for discussions.

Appendix

In order to make quantitative comparisons between the experiments described in § 2 and the steady-state model developed in § 3, we need to constrain the model parameters λ and c which quantify the efficiency of the heat transfer from the heated plate and the energy loss through the doorway associated with the displacement flow, respectively. We have therefore conducted two series of controlled calibration experiments.

A.1. *Displacement ventilation*

In the first calibration experiments, we examined the rate of ascent of a saline–fresh water interface inside the room driven as a pure displacement flow, to identify the value of the constant c from equation (3.6) for our experimental apparatus. The fluid inside the room was initially fresh, while the external flow was a denser aqueous saline solution. Extending the model of the displacement flow from equation (3.1), the rate

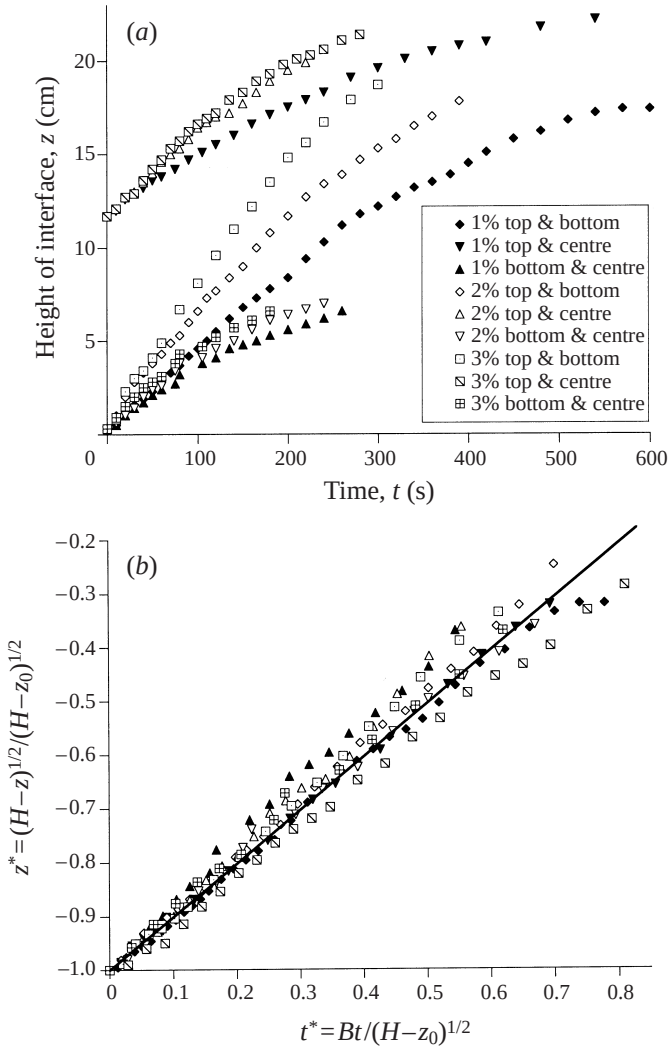

FIGURE 10. (*a*) The interface height, z, is traced with time, t, during transient displacement ventilation of saline and fresh water for calibration experiments using different configurations of openings and varying initial salinities. (*b*) Scaled transient displacement ventilation data collapse to a straight line. The slope gives a value for the constant c from equation (3.6) of $c = 0.98 \pm 0.15$.

of ascent of the interface, z, is given by

$$A_R \frac{\mathrm{d}z}{\mathrm{d}t} = cA_H \left[g' \frac{(h-z)}{2} \right]^{1/2} \tag{A 1}$$

where the reduced gravity $g' = g(\rho_{ext} - \rho_{int})/\rho_{int}$, A_R and A_H are the area of the room and the average area of the openings respectively and h is the distance between the openings. This can be integrated to give

$$(h-z_0)^{1/2} - (h-z)^{1/2} = cBt \quad \text{where} \quad B = \left(\frac{A_H}{A_R} \right) \frac{g'^{1/2}}{2\sqrt{2}} \tag{A 2}$$

and z_0 is the initial height of the interface.

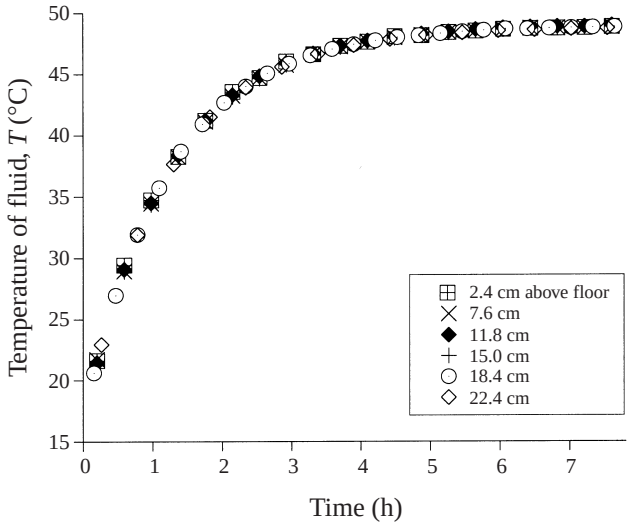

FIGURE 11. During transient heating calibration experiments all interior thermocouples give the same temperature increase with time from $T_E = 15\,^{\circ}\mathrm{C}$ at $t = 0$ towards $T_F = 50\,^{\circ}\mathrm{C}$ indicating that the fluid is well-mixed.

During transient displacement ventilation experiments, the room is filled with dyed fresh water and the exterior reservoir filled with 1%, 2% or 3% saline solution by mass. Stoppers are removed from two of the three available openings. There are three configurations of openings: (i) top and bottom, (ii) top and central, and (iii) central and bottom stoppers are removed. The light interior fluid then flows out of the room through the upper opening while dense exterior fluid flows into the room through the lower opening. There is a substantial amount of mixing during initial stages of an experiment when the dense fluid enters the room. To reduce the impact of this on visualization of the interface, the basal portion of the room is filled with a layer of saline solution identical in concentration to that outside the room. This basal layer typically extends to 2 cm above the lower opening. The ascending interface between these two fluids is monitored with time using Digimage (Dalziel 1993) image analysis software. Twelve experiments were performed, using three configurations of openings and three salinities; three experiments were repeated.

The interface between the two fluids rises with time although the rate of ascent decreases with time (figure 10*a*). The interface rises more rapidly where there is a large density difference between the two fluids. These observations concur with those made by Linden *et al.* (1990).

In figure 10(*b*) we scale our experimental data on $(h - z_0)^{1/2}$ using equation (A 2) so that the dimensionless height of the interface, z^*, and dimensionless time, t^*, are

$$z^* = \frac{-(h-z)^{1/2}}{(h-z_0)^{1/2}} \quad \text{and} \quad t^* = \frac{Bt}{(h-z_0)^{1/2}}. \tag{A 3}$$

Using these scalings, the data for all configurations of openings and salinities collapse to a line with a slope giving a value of $c = 0.98 \pm 0.15$ (figure 10*b*). This suggests that as fluid moves through an opening it expands comparatively smoothly and hence loses little energy (Batchelor 1967).

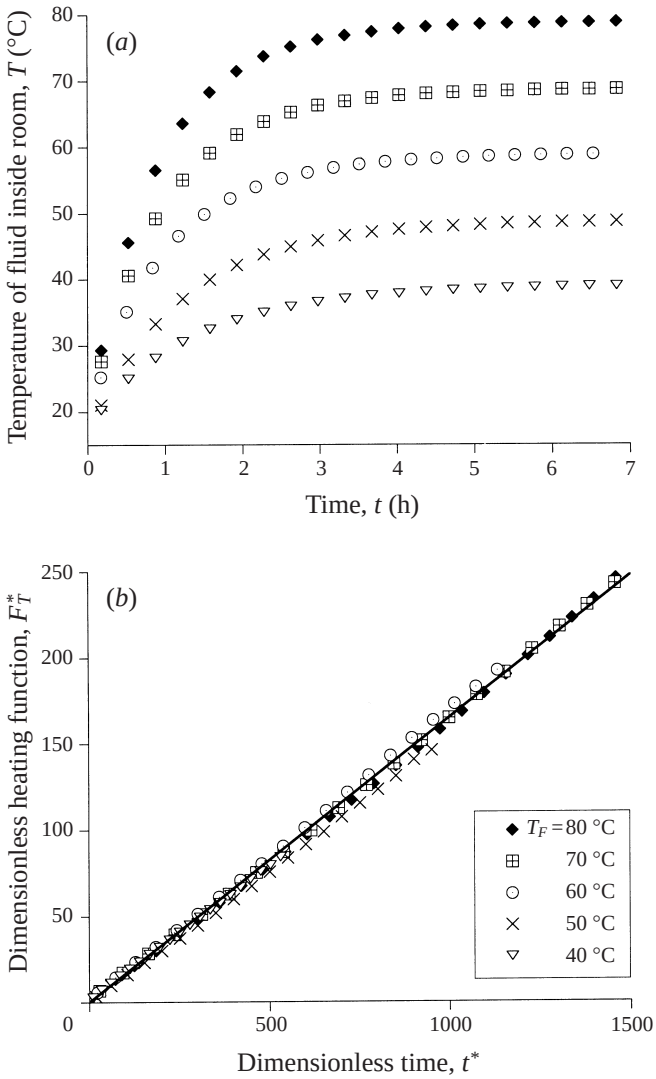

FIGURE 12. (*a*) Transient heating experiments are conducted using increasing values of T_F from 40 °C to 80 °C. Each curve represents an average of all interior thermocouples, and shows that T increases rapidly at first and then more gradually with time. (*b*) Transient heating data are scaled using equations (A 6) and (A 7). The slope of the best-fit line gives a value for the heating plate coefficient of $\lambda = 0.166 \pm 0.003$, required for the steady-state model described by equation (3.6).

A.2. *Transient heating*

The second calibration experiment involved heating the closed room by the floor plate and measuring the temperature of the room as a function of time, so as to identify the value of the coefficient λ from equation (3.2) for our heating plate. From (3.2), the change in temperature of fluid in the closed room, T, becomes,

$$\frac{\mathrm{d}T}{\mathrm{d}t} = \lambda J_T (T_F - T)^{4/3} \tag{A 4}$$

where T_F is the temperature of the floor and

$$J_T = \left(\frac{\alpha\kappa^2 g}{\nu}\right)^{1/3} \frac{1}{H}, \tag{A 5}$$

where H is the depth of the fluid.

During transient heating experiments, the room was insulated on all sides including the floor and top, and the heating plate comprising the floor was preheated to T_F. We conducted experiments using values for T_F of 40, 50, 60, 70 and 80 °C. In all experiments, the room was filled with water with initial temperature, $T_E = 15$ °C. The temperature inside the room was monitored using thermocouples at seven vertical heights until T reached T_F. In each experiment, we find that the fluid inside the room increases in temperature T, rapidly at first as then more gradually as T approaches T_F (figure 11). All thermocouples, independent of vertical position within the room, show the same increase in T, indicating that the room is well-mixed. Typically it takes five to eight hours for T to reach T_F. The rate of temperature increase depends upon T_F (figure 12*a*), with higher values of T_F producing more rapid increases of T during early stages of an experiment than lower values. As T_E was constant in all experiments, T only depends on T_F.

Integrating and scaling equation (A 4) provides expressions for a dimensionless heating function, $F_T{}^*$, with dimensionless time, t^*:

$$F_T{}^* = [J_T(T_F - T_E)^{4/3}] \int_{T_E}^{T} \frac{1}{J_T(T_F - T)^{4/3}} \mathrm{d}T, \tag{A 6}$$

$$t^* = [J_T(T_F - T_E)^{4/3}]t. \tag{A 7}$$

In figure 12(*b*), $F_T{}^*$ and t^* are plotted for each experiment until $T = 0.95T_F$. Using this scaling gives an excellent collapse to a line with slope of value λ where $\lambda = 0.166 \pm 2\%$. Thus the heat transfer coefficient c_q is 0.066. This compares well with previous observations for both single-plate (e.g. Townsend 1959) and double-plate (e.g. Garon & Goldstein 1973; Denton & Wood 1979) turbulent convection experiments.

REFERENCES

Alamdari, F., Butler, D. J. G., Gridd, P. F. & Shaw, M. R. 1998 Chilled ceilings and displacement ventilation. *Renewable Energy* **15**, 300–305.

Allard, F. 1998 *Natural Ventilation in Buildings: a Design Handbook*. James & James Ltd.

Awbi, H. B. 1991 *Ventilation of Buildings*. Chapman & Hall.

Batchelor, G. K. 1967 *An Introduction to Fluid Dynamics*. Cambridge University Press.

Castaing, B., Gunaratne, G., Heslot, F., Kadanoff, L., Libchaber, A., Thomae, S., Wu, X. Zaleski, S. & Zanetti, G. 1989 Scaling of hard thermal turbulence in Rayleigh-Benard convection. *J. Fluid Mech.* **204**, 1–30.

Chen, Q. & Glicksman, L. 2001 Application of computational fluid dynamics for indoor air quality studies. In *Air Quality Handbook*. McGraw-Hill.

Cooper, P. & Linden, P. F. 1996 Natural ventilation of an enclosure containing two buoyancy sources. *J. Fluid Mech.* **311**, 153–176.

Dalziel, S. B. 1993 Rayleigh-Taylor instability: experiments with image analysis. *Dyn. Atmos. Oceans* **20**, 127–153.

Dalziel, S. B. & Lane-Serff, G. F. 1991 The hydraulics of doorway exchange flows. *Building Environ.* **26**, 121–135.

Denton, R. A. & Wood, I. R. 1979 Turbulent convection between two horizontal plates. *Intl J. Heat Mass Transfer* **22**, 1339–1346.

Etheridge, D. & Sandberg, M. 1996 *Building Ventilation – Theory and Measurement*. John Wiley & Sons.

Garon, A. M. & Goldstein, R. J. 1973 Velocity and heat transfer measurements in thermal convection. *Phys. Fluids* **16**, 1818–1825.

Gladstone, C. & Woods, A. W. 2000 A hybrid displacement-mixing ventilation regime in a naturally ventilated room. In *Proc. Roomvent 2000: 7th Intl Conf. on Air Distribution in Rooms, Reading, UK* (ed. H. B. Awbi), pp. 259–264. Elsevier.

Holford, J. M. & Hunt, G. R. 2000 Multiple steady states in natural ventilation. In *Proc. 5th Intl Symp. on Stratified Flows, Vancouver* (ed. G. A. Lawrence, R. Pieters & N. Yonomitsu), pp. 661–666.

Hunt, G. R. & Linden, P. F. 1999 The fluid mechanics of natural ventilation – displacement ventilation by buoyancy-driven flows assisted by wind. *Building Environ.* **34**, 707–720.

Hunt, G. R. & Linden, P. F. 2000 Multiple steady airflows and hysteresis when wind opposes buoyancy. *Air Infiltration Review*, vol. 21, no. 2, March 2000.

Kerr, R. C., Woods, A. W., Worster, M. G. & Huppert, H. E. 1990 Solidification of an alloy cooled from above. Part 1. Equilibrium growth. *J. Fluid Mech.* **216**, 323–342.

Linden, P. F. 1999 The fluid mechanics of natural ventilation. *Ann. Rev. Fluid Mech.* **31**, 201–238.

Linden, P. F., Lane-Serff, G. F. & Smeed, D. A. 1990 Emptying filling boxes: the fluid mechanics of natural ventilation. *J. Fluid Mech.* **212**, 309–335.

Phillips, J. C. & Woods, A. W. 2000 Natural ventilation of an enclosed room by doorway exchange flows. In *Proc. Roomvent 2000: 7th Intl Conf. on Air Distribution in Rooms, Reading, UK* (ed. H. B. Awbi), pp. 253–258. Elsevier.

Sandberg, M. & Lindström, S. 1990 Stratified flow in ventilated rooms – a model study. In *Proc. Roomvent '90: 2nd Intl Conf. on Air Distribution in Rooms, Oslo, Norway*.

Thomas, P. H., Hinkley, P. L., Theobald, C. R. & Simms, D. L. 1963 Investigations into the flow of hot gases in roof venting. *Fire Res. Tech. Paper* 7. HMSO.

Townsend, A. A. 1959 Temperature fluctuations over a heated horizontal surface. *J. Fluid Mech.* **5**, 209–241.

Turner, J. S. 1973 *Buoyancy Effects in Fluids*. Cambridge University Press.

Weast, R. A. 1987 *CRC Handbook of Chemistry and Physics*. CRC Press.